Roles of laser ellipticity in attoclocks

J. Y. Che,[1,*] J. Y. Huang,[1,*] F. B. Zhang,[1] C. Chen,[1,†] G. G. Xin,[2] and Y. J. Chen[1,‡]
[1]*College of Physics and Information Technology, Shaan'xi Normal University, Xi'an 710119, China*
[2]*School of Physics, Northwest University, Xi'an 710127, China*

(Received 30 January 2023; accepted 29 March 2023; published 11 April 2023)

We study ionization of atoms in strong elliptically polarized laser fields numerically and analytically. We focus on the effects of laser ellipticity on the offset angle in the photoelectron momentum distribution. This angle is considered to encode the time information of tunneling ionization in attoclock experiments. The calculated offset angle increases with the decrease of ellipticity, but the momentum along the major axis of laser polarization related to this angle changes slowly, in agreement with experiments. With a Coulomb-included strong-field model, the scaling laws for the ellipticity dependence of this angle and relevant momentum components are obtained, and the ellipticity dependence of Coulomb-induced ionization time lag encoded in this angle is also addressed.

DOI: 10.1103/PhysRevA.107.043109

I. INTRODUCTION

The development of ultrafast and ultrastrong laser technology provides the opportunity for probing the motion of an electron inside an atom or a molecule at its natural scale [1–7]. Relevant probing procedures use photoelectron spectra [8,9] or harmonic spectra [10,11] generated by the strong interaction between the laser and matter. An attoclock is such a procedure which uses the offset angle in the photoelectron momentum distribution (PMD) generated by ionization of the gas target in strong elliptical laser fields to probe tunneling dynamics [12–14]. Many actual and numerical experiments on attoclocks have been performed for different targets and laser parameters [15–21]. Some interesting parameter-dependent phenomena have been revealed. For example, it was shown that the offset angle increases with the decrease of laser intensity [22]. This typical phenomenon has attracted much theoretical attention in recent years. Many efforts have been devoted to developing applicable Coulomb-included strong-field models to quantitatively explain this phenomenon. Relevant studies provide deep insights into different aspects of strong-laser-induced tunneling, including the time delay of the tunneling electron under the barrier [22], nonadiabatic effects [23], and classical scattering [24] at the tunnel exit.

Besides laser intensity, the laser wavelength and ellipticity can also play a nontrivial role in attoclocks. Due to the uncertainty in calibrating the laser intensity in experiments, studies on ellipticity-dependent phenomena in attoclocks provide a beneficial complement to intensity-dependent ones [23]. Recent experiments have reported ellipticity-resolved studies on momentum distributions generated by strong-field ionization of He [25,26]. These studies focus on the influence of the Coulomb potential on the longitudinal momentum spread of the electron wave packet at the tunnel exit [25] and on the momenta related to the offset angle in the PMD [26]. It has been shown that the studied Coulomb effects are more remarkable for cases of small ellipticity than cases of high ellipticity. In comparison with studies on laser intensity, systematic experimental and theoretical studies on the effects of laser ellipticity and wavelength on attoclocks are relatively fewer at present.

In this paper we study ionization of the He atom in strong elliptically polarized laser fields theoretically. By changing the laser ellipticity at different laser wavelengths, we explore the ellipticity-related effects on the offset angle in the PMD. This angle is the main observable which is used to deduce the time-domain information on tunneling in attoclocks. Our simulations are performed through the numerical solution of the time-dependent Schrödinger equation (TDSE), and we describe single-electron ionization dynamics in both two-dimensional (2D) and three-dimensional (3D) cases.

Our results show that when the laser ellipticity increases, the offset angle becomes smaller. For a certain ellipticity, this angle is larger for shorter laser wavelengths. By contrast, for the momentum components related to the offset angle, the component along the major axis of laser polarization (denoted p_x in this paper) is not sensitive to the ellipticity and the wavelength, suggesting that these angle-related phenomena arise from the dependence of the momentum component along the minor polarization axis (denoted p_y here) on ellipticity and wavelength. These ellipticity-dependent phenomena are well described by a strong-field response-time model which attributes the complex Coulomb effect to an ionization time lag (i.e., the response time of the electron to light). With this model, we are able to quantitatively analyze the roles of ellipticity in the momentum (p_x, p_y) and the offset angle, as well as in the Coulomb-induced ionization time lag which is related mainly to the momentum component p_x and is encoded in the offset angle.

*These authors contributed equally to this paper.
†chenchao1202@163.com
‡chenyjhb@gmail.com

II. THEORY METHODS

Numerical methods. In our simulations, we choose the He atom as the target. In the single-active electron approximation and the length gauge, the Hamiltonian of the model He system interacting with a strong laser field can be written as (in atomic units of $\hbar = e = m_e = 1$)

$$H(t) = H_0 + \mathbf{E}(t) \cdot \mathbf{r}. \tag{1}$$

Here, $H_0 = \mathbf{p}^2/2 + V(\mathbf{r})$ is the field-free Hamiltonian, and $V(\mathbf{r}) = -Z/\sqrt{r^2 + \xi}$ is the Coulomb potential with effective charge Z and the soft-core parameter ξ. The term $\mathbf{E}(t)$ denotes the electric field of the laser. In 2D cases, we use $Z = 1.45$ and $\xi = 0.5$. With these parameters, the ionization potential of the model system reproduced here is $I_p = 0.9$ a.u. In 3D cases, those parameters are $Z = \sqrt{2I_p} \approx 1.34$ and $\xi = 0.071$.

In elliptically polarized cases, the electric field $\mathbf{E}(t)$ used here has the form of $\mathbf{E}(t) = f(t)[\vec{\mathbf{e}}_x E_x(t) + \vec{\mathbf{e}}_y E_y(t)]$, with $E_x(t) = E_0 \sin(\omega t)$ and $E_y(t) = E_1 \cos(\omega t)$, where $E_0 = E_L/\sqrt{1+\varepsilon^2}$ and $E_1 = \varepsilon E_L/\sqrt{1+\varepsilon^2}$. Here, E_L is the maximal laser amplitude corresponding to the peak intensity I, ε is the ellipticity, ω is the laser frequency, and $f(t)$ is the envelope function. The term $\vec{\mathbf{e}}_x$ ($\vec{\mathbf{e}}_y$) is the unit vector along the x (y) axis. We use trapezoidally shaped laser pulses with a total duration of 15 cycles which are linearly turned on and off for 3 optical cycles and then kept at a constant intensity for 9 additional cycles. The TDSE of $i\dot{\Psi}(\mathbf{r}, t) = H(t)\Psi(\mathbf{r}, t)$ is solved numerically using the spectral method [27] with a time step of $\triangle t = 0.05$ a.u. In 2D cases, we use a grid size of $L_x \times L_y = 409.6 \times 409.6$ a.u. with space steps of $\triangle x = \triangle y = 0.4$ a.u. In 3D cases, the grid size is $L_x \times L_y \times L_z = 358.4 \times 358.4 \times 51.2$ a.u. with $\triangle x = \triangle y = 0.7$ a.u. and $\triangle z = 0.8$ a.u.. The numerical convergence is checked by using a finer grid.

In order to avoid the reflection of the electron wave packet from the boundary and obtain the momentum-space wave function, the coordinate space is split into inner and outer regions with $\Psi(\mathbf{r}, t) = \Psi_{\text{in}}(\mathbf{r}, t) + \Psi_{\text{out}}(\mathbf{r}, t)$ by multiplication using a mask function $F(\mathbf{r})$. In 2D cases, the mask function has the form $F(\mathbf{r}) = F(x, y) = \cos^{1/2}[\pi(r_b - r_f)/(L_r - 2r_f)]$ for $r_b \geqslant r_f$ and $F(x, y) = 1$ for $r_b < r_f$. Here, $r_b = \sqrt{x^2 + y^2/\varepsilon^2}$, and $r_f = 2.1x_q$, with $x_q = E_0/\omega^2$; $L_r/2 = r_f + 50$ a.u., with $L_r \leqslant L_x$. The above procedure considers the fact that the quiver amplitude of the ionized electron differs for different laser parameters and for the x and y directions. In 3D cases, the mask function is $F(\mathbf{r}) = F_1(x, y)F_2(z)$. The expression for $F_1(x, y)$ is similar to that for $F(x, y)$ used in the 2D cases. The expression for $F_2(z)$ is $F_2(z) = \cos^{1/2}[\pi(|z| - r_z)/(L_z - 2r_z)]$ for $|z| \geqslant r_z$ and $F_2(z) = 1$ for $|z| < r_z$. Here, $r_z = 19.2$ a.u. is the absorbing boundary along the z direction. In the inner region, the wave function $\Psi_{\text{in}}(\mathbf{r}, t)$ is propagated with the complete Hamiltonian $H(t)$. In the outer region, the time evolution of the wave function $\Psi_{\text{out}}(\mathbf{r}, t)$ is carried out in momentum space with the Hamiltonian of the free electron in the laser field. The mask function is applied at each time interval of 0.5 a.u., and the obtained fractions of the outer wave function are added to the momentum-space wave function $\tilde{\Psi}_{\text{out}}(\mathbf{r}, t)$ from which we obtain the PMD. Then we find the local maximum in the upper half plane of the PMD, and the offset angle θ is obtained with the local maximum.

Analytical methods. To analytically study the ionization of atoms in strong elliptical laser fields, we use a model called the tunneling-response-classical-motion (TRCM) model which gives an applicable description of the intensity-dependent offset angle [28]. The TRCM arises from strong-field approximation (SFA) [29] but considers the Coulomb effect [30–32].

SFA description. First, according to the SFA with the saddle-point method [9,29], strong-field ionization is characterized by tunneling, and each photoelectron drift momentum $\mathbf{p}$ has a corresponding tunneling-out time t_0, in agreement with the following mapping relation:

$$\mathbf{p} \equiv \mathbf{p}(t_0) = \mathbf{v}(t_0) - \mathbf{A}(t_0). \tag{2}$$

Here, $\mathbf{A}(t)$ is the vector potential of the electric field $\mathbf{E}(t)$. The tunneling-out time t_0 is the real part of the complex time $t_s = t_0 + it_x$ that satisfies the saddle-point equation $[\mathbf{p} + \mathbf{A}(t_s)]^2/2 = -I_p$. Without considering the Coulomb potential, the tunneling-out time t_0 also corresponds to the ionization time at which the electron is free. The term $\mathbf{v}(t_0) = \mathbf{p} + \mathbf{A}(t_0)$ denotes the exit velocity of the photoelectron at the exit position (i.e., the tunnel exit) $\mathbf{r}_0 \equiv \mathbf{r}(t_0) = \text{Re}\{\int_{t_s}^{t_0}[\mathbf{p} + \mathbf{A}(t')]dt'\}$ [32]. This velocity reflects the basic quantum effect of tunneling. The momentum-time pair $(\mathbf{p}, t_0)$ has been termed the electron trajectory. The corresponding complex amplitude for the trajectory $(\mathbf{p}, t_0)$ can be expressed as $c(\mathbf{p}, t_0) \sim e^b$. Here, b is the imaginary part of the quasiclassical action $S(\mathbf{p}, t_s) = \int_{t_s}\{[\mathbf{p} + \mathbf{A}(t')]^2/2 + I_p\}dt'$, with $t_s = t_0 + it_x$ [29].

TRCM description. Around the tunnel exit $r_0 = |\mathbf{r}_0|$, which is about 10 a.u. away from the nucleus for the general laser and atomic parameters used in experiments, the high-energy bound eigenstate of H_0 has large probability amplitudes. The TRCM therefore assumes that for an actual atom with long-range Coulomb potential, at the tunnel exit $\mathbf{r}(t_0)$, the tunneling electron with the drift momentum $\mathbf{p}$ predicted by SFA is still located in a quasibound state. This state is characterized by an electron wave packet consisting of high-energy bound eigenstates of H_0 and approximately agrees with the virial theorem. A small period of time τ is needed for the tunneling electron to evolve from the quasibound state into an ionized state. Then it is free at time $t_i = t_0 + \tau$ with the Coulomb-included drift momentum $\mathbf{p}'$. This time τ can be understood as the response time of the electron to light in laser-induced photoelectric effects and manifests as the Coulomb-induced ionization time lag in strong-field ionization [33,34]. The mapping between the drift momentum $\mathbf{p}'$ and the ionization time t_i in the TRCM is expressed as

$$\mathbf{p}' \equiv \mathbf{p}'(t_i) = \mathbf{v}(t_0) - \mathbf{A}(t_i). \tag{3}$$

Angle formula. The offset angle θ in the PMD is related to the most probable route (MPR), which corresponds to the momentum having the maximal amplitude in the PMD. For the MPR, the tunneling-out time t_0 of the photoelectron agrees with the peak time of the laser field. This angle θ satisfies the following relation:

$$\tan\theta = p'_x/p'_y = A_x(t_i)/[A_y(t_i) - v_y(t_0)]. \tag{4}$$

The above expression considers the fact that for the MPR $v_x(t_0) = 0$. By neglecting $v_y(t_0)$, the adiabatic version of the

above expression is also obtained. That is,

$$\tan\theta \approx A_x(t_i)/A_y(t_i). \tag{5}$$

The adiabatic version is applicable for $\gamma \ll 1$, with $\gamma = w\sqrt{2I_p}/E_0$ being the Keldysh parameter [35]. It was used in [36] to deduce the lag τ of the asymmetric system HeH^+ and was termed the Coulomb-calibrated attoclock (CCAC). In the CCAC, while considering $t_i = t_0 + \tau$ and $\omega t_0 = \pi/2$ for the MPR, we can further obtain the following relation:

$$\tan\theta \approx \tan(\omega\tau)/\varepsilon \approx \theta \approx \omega\tau/\varepsilon \tag{6}$$

for a small angle θ. With the above expressions, when the lag $\tau = t_i - t_0$ is obtained analytically or numerically, one can further obtain the offset angle θ. In turn, when the angle θ is obtained in experiments or TDSE simulations, one can also deduce the lag τ from this angle.

Lag formula. According to the assumptions in the TRCM model, at the tunneling-out time t_0, the electron is still located in a quasibound state ψ_b which approximately agrees with the virial theorem. The average potential energy of this state is $\langle V(\mathbf{r})\rangle \approx V(\mathbf{r}(t_0))$, and the average kinetic energy is $\langle \mathbf{v}^2/2\rangle = n_f\langle v_x^2/2\rangle \approx -V(\mathbf{r}(t_0))/2$. This Coulomb-induced velocity $|v_x| \approx \sqrt{|V(\mathbf{r}(t_0))|/n_f}$ reflects the basic symmetry requirement of the Coulomb potential in the electronic state. A time lag τ is needed for the tunneling electron to acquire an impulse from the laser field in order to break this symmetry. Then for the MPR, the lag τ can be evaluated with the expression $\tau \approx \sqrt{|V(\mathbf{r}(t_0))|/n_f}/E_0$. Here, $n_f = 2, 3$ is the dimension of the system studied, and the exit position $\mathbf{r}(t_0)$ is determined by the saddle points, as discussed above. For a hydrogenlike atom in the form of the Coulomb potential $V(\mathbf{r}) = -Z/r$, by neglecting the field $E_y(t)$ in the solution of the saddle-point equation, an approximate expression for τ can also be obtained. That is,

$$\tau \approx \sqrt{Z\omega^2/\left[n_f E_0^3(\sqrt{\gamma^2+1}-1)\right]}. \tag{7}$$

For real 3D cases such as in experiments, the value of the effective charge Z can be evaluated with $Z = \sqrt{2I_p}$. For the 2D TDSE, the value of Z can be chosen to be that used in simulations. Similarly, an approximate expression for $v_y(t_0)$ can also be obtained. That is,

$$v_y(t_0) = [\varepsilon\sqrt{2I_p}/\mathrm{arcsinh}(\gamma) - E_1/\omega]\sin\omega t_0. \tag{8}$$

By inserting Eqs. (7) and (8) into Eq. (4), we can analytically evaluate the offset angle θ. In this paper, we call the above manner for obtaining θ the TRCM. Similarly, by inserting Eq. (7) into Eq. (6), the adiabatic prediction of the angle θ can also be obtained, and this method can be called the CCAC.

PMDs. In the TRCM treatment, by assuming that for an arbitrary SFA electron trajectory $(\mathbf{p}, t_0)$, the Coulomb potential does not influence the corresponding complex amplitude $c(\mathbf{p}, t_0)$, we can obtain the TRCM amplitude $c(\mathbf{p}', t_i)$ for the Coulomb-included electron trajectory $(\mathbf{p}', t_i)$ directly from the SFA one with $c(\mathbf{p}', t_i) \equiv c(\mathbf{p}, t_0)$ at $\tau \approx \sqrt{|V(\mathbf{r}(t_0))|/n_f}/|\mathbf{E}(t_0)|$. This TRCM therefore allows analytical evaluation of the Coulomb-included PMD without the need to solve Newton's equation including both the electric force and the Coulomb force. The TRCM prediction of the PMD for He is presented in the right column of Fig. 1.

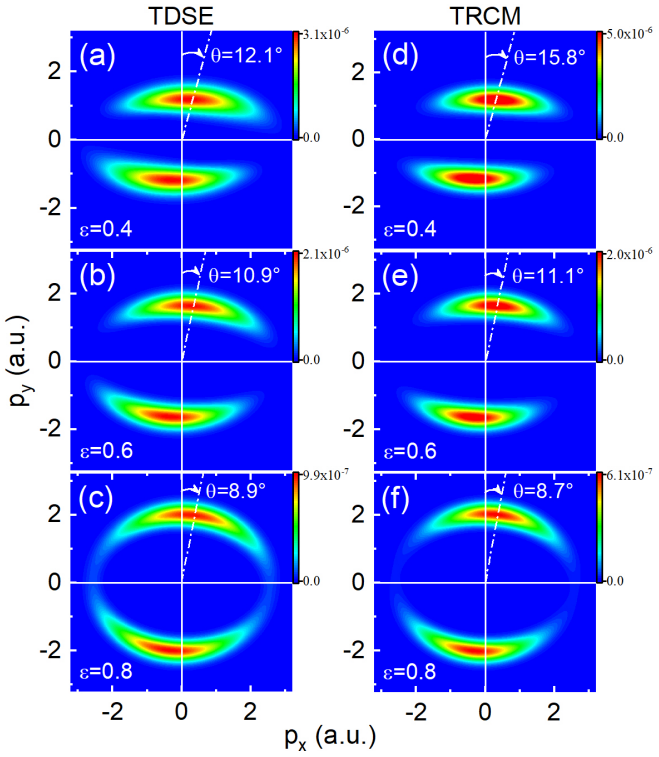

FIG. 1. PMDs of He obtained with the 2D TDSE (left column) and TRCM (right) at different laser ellipticities ε. Laser parameters are $I = 7\times10^{14}$ W/cm^2 and $\lambda = 1000$ nm. The laser ellipticity is as shown. The offset angle θ related to the momentum with the maximal amplitude in PMD is also indicated in each panel.

III. RESULTS AND DISCUSSION

Two-dimensional cases. We first present our comparisons of the TDSE and TRCM in 2D cases which allow us to explore a wide parameter region. In Fig. 1, we present PMDs of He obtained with the TDSE and TRCM in strong elliptical laser fields with different ε. The offset angle in the PMD of the TDSE decreases with the increase of ellipticity, as seen in the left column of Fig. 1. This decreasing trend is well reproduced by the TRCM, as seen in the right column of Fig. 1. For a relatively large ellipticity of $\varepsilon \geqslant 0.6$, the TRCM offset angle in the PMD is also in quantitative agreement with the corresponding TDSE one. For the case of $\varepsilon = 0.4$ in the first row of Fig. 1, the TRCM result is about 4° larger than the TDSE one, suggesting that the TRCM is more applicable for the case of relatively large ellipticity. We will return to this point later.

Roles of ε. In Fig. 2, we further show comparisons of the offset angle and the momentum (p_x, p_y), which is associated with this angle and has the maximal amplitude in the PMD, for diverse laser ellipticities and wavelengths. Without loss of generality, in this paper, we consider the cases of the momentum (p_x, p_y) to be located in the first quadrant of the PMD with $p_x > 0$, $p_y > 0$.

First, for the momentum p_y along the minor axis of polarization, one can see from Fig. 2(a) that the TDSE and TRCM results agree well with each other. The TDSE and TRCM predictions of p_x along the major axis of polarization deviate remarkably from each other for the case of small ellipticity

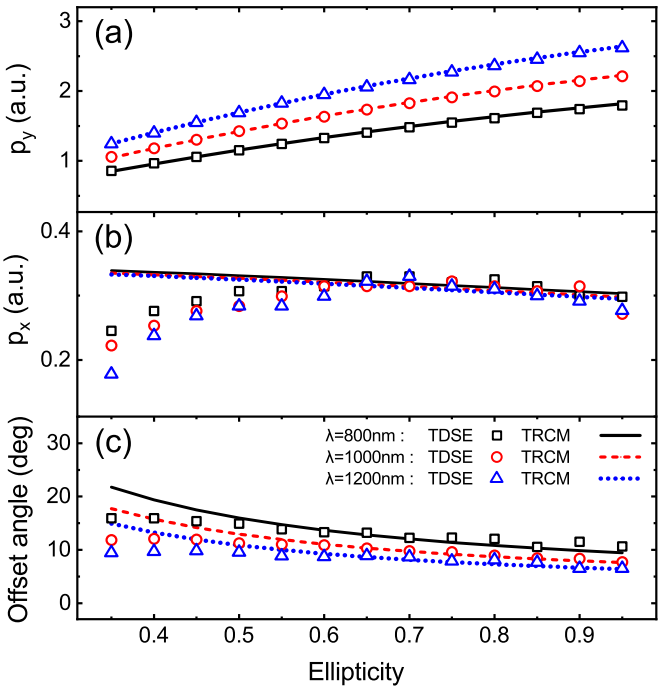

FIG. 2. Comparisons of the drift momentum (p_x, p_y) related to the MPR and the offset angle θ for the 2D TDSE and TRCM from Eq. (4) at different laser ellipticities ε and wavelengths λ. The laser intensity is $I = 7 \times 10^{14}$ W/cm^2.

$\varepsilon \leqslant 0.4$ and become close to and coincident with each other for intermediate and larger ellipticities, as seen in Fig. 2(b). Accordingly, in Fig. 2(c), the angles predicted by the TDSE and TRCM also show a remarkable difference for small ellipticity and agree with each other at larger ellipticity with $\varepsilon \geqslant 0.5$. This remarkable difference between the TRCM and TDSE could arise for the following reason. For small ellipticity, an ionized electron wave packet related to a rescattering electron trajectory can interfere with a wave packet related to a direct-ionization electron trajectory [9]. This interference will influence the amplitude of the PMD and therefore influence the identification of the offset angle. These influences are not considered in the TRCM.

It is also worth noting that in Fig. 2, for the region of $0.6 \leqslant \varepsilon \leqslant 0.95$, in which the TRCM works well, the momentum p_x decreases slowly with the increase of ellipticity. By contrast, the momentum p_y increases remarkably with increasing ellipticity. One therefore can expect that in this region, the dependence of the momentum p_y on ellipticity plays a more important role in the ellipticity dependence of the offset angle $\theta \approx p_x/p_y$.

Scaling laws. With the TRCM, we can also obtain different scaling laws for the dependence of momentum components p_x and p_y on the ellipticity ε. Using Eq. (5) for the adiabatic approximation that is applicable for a small Keldysh parameter, we have $p_y \approx A_y(t_0) \approx \varepsilon E_0/\omega$ and $p_x \approx A_x(t_i) \approx E_0\tau \approx \sqrt{|V(\mathbf{r}(t_0))|/n_f}$. By considering $V(r) = -Z/r$, $r(t_0) \approx I_p/E_0$, and $E_0 = E_L/\sqrt{1+\varepsilon^2}$, we also have

$$p_x \approx \sqrt{ZE_L/(n_f I_p\sqrt{1+\varepsilon^2})} = A(1+\varepsilon^2)^{-1/4} \tag{9}$$

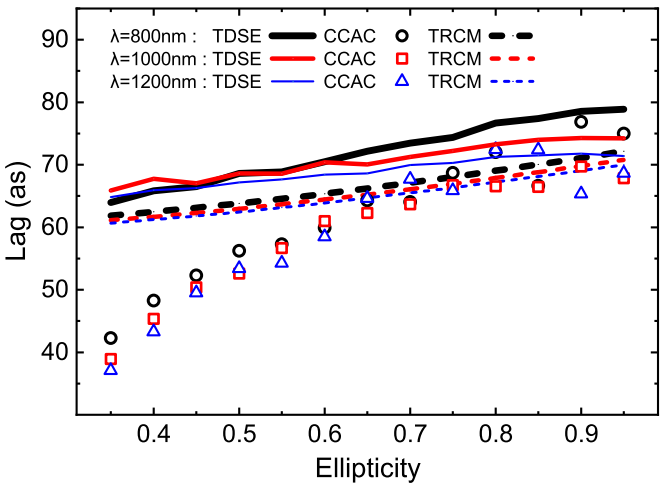

FIG. 3. Comparisons of the time lag τ for the 2D TDSE, CCAC, and TRCM from Eq. (7) at different laser ellipticities ε and wavelengths λ. The TDSE results are obtained by finding the peak time of the instantaneous ionization rate. The CCAC results are obtained by deducing the lag τ from the TDSE offset angle θ with $\tau \approx \varepsilon\theta/\omega$ from Eq. (6). The laser intensity is $I = 7 \times 10^{14}$ W/cm^2.

and

$$p_y \approx \varepsilon E_L/(\omega\sqrt{1+\varepsilon^2}) = B\varepsilon(1+\varepsilon^2)^{-1/2}. \tag{10}$$

Here, $A \equiv A(E_L, I_p) = \sqrt{ZE_L/(n_f I_p)}$, with $Z = \sqrt{2I_p}$, which is independent of the frequency ω, and $B \equiv B(E_L, \omega) = E_L/\omega$, which is independent of the ionization potential I_p. Then we obtain the scaling laws for the momentum (p_x, p_y) with

$$p_x \sim (1+\varepsilon^2)^{-1/4}, \quad p_y \sim \varepsilon(1+\varepsilon^2)^{-1/2}. \tag{11}$$

For the parameter region with $0.3 \leqslant \varepsilon \leqslant 1$ explored in this paper, we have $0.98A \geqslant p_x \geqslant 0.84A$ and $0.29B \leqslant p_y \leqslant 0.71B$, which indicate the slow decrease of p_x and the remarkable increase of p_y with the increase of ε observed in Figs. 2(b) and 2(a), respectively. Equations (9) and (10) also shed light on the different responses of p_x and p_y to the laser wavelength λ seen in Fig. 2.

With Eqs. (9) and (10), we can also obtain the scaling law for the ellipticity-dependent angle θ with $\theta \approx p_x/p_y$ and $p_y \neq 0$. That is,

$$\theta \approx C(1+\varepsilon^2)^{1/4}\varepsilon^{-1} \sim (1+\varepsilon^2)^{1/4}\varepsilon^{-1}. \tag{12}$$

Here, $C \equiv C(E_L, I_p, \omega) = \omega\sqrt{Z/(n_f I_p E_L)}$. Equation (12) provides an explanation for the ellipticity-wavelength-related phenomena in Fig. 2(c).

Considering $p_x \approx E_0\tau$ and Eq. (9), we can also obtain the relevant scaling law for the lag τ. That is,

$$\tau \approx D(1+\varepsilon^2)^{1/4} \sim (1+\varepsilon^2)^{1/4}. \tag{13}$$

Here, $D \equiv D(E_L, I_p) = \sqrt{Z/(n_f I_p E_L)}$. Equation (13) shows that the lag slowly increases with increasing ellipticity and can be used to analyze ellipticity-dependent phenomena for the lag τ, as shown in Fig. 3.

Let us discuss the derivation of the scaling laws. First, according to the TRCM, we can obtain the general expression for momenta p_x and p_y, as shown in Eq. (3). Then we can

deduce the scaling laws of momenta p_x and p_y and angle θ for the most probable electron trajectory (i.e., the MPR). The MPR is related to the peak time t_0 of the fundamental field $E_x(t)$ and implies the condition $v_x(t_0) = 0$. Recent studies have reported that for large Keldysh parameters (larger than 1), the PMD shows remarkable photon rings [37–39] and the offset angles in different rings differ from each other [38]. For our cases of high laser intensities and long wavelengths corresponding to small Keldysh parameters (smaller than 1), the rings are not resolvable, and we focus our discussion on only the MPR.

Second, the adiabatic condition of $v_y(t_0) \approx 0$ is also considered for the case of p_y which holds when the Keldysh parameter is far less than 1. Then we arrive at Eq. (5), from which we can obtain the additional expressions $p_x \approx A_x(t_0 + \tau) \approx E_0\tau \approx \sqrt{|V(\mathbf{r}(t_0))|/n_f}$ and $p_y \approx A_y(t_0 + \tau) \approx \varepsilon E_0/\omega$. These expressions consider the TRCM lag formula $\tau \approx \sqrt{|V(\mathbf{r}(t_0))|/n_f}/E_0$ above Eq. (7) and produce the scaling laws in Eqs. (11) and (12). Because for the MPR and small values of the Keldysh parameter the exit position agrees with the relation $r(t_0) \approx I_p/E_0$ independent of the laser frequency, the above expressions for p_x and p_y show that when the value of p_y depends strongly on the laser frequency (wavelength), the value of p_x is not sensitive to that, in agreement with the observation in Fig. 2.

Third, the lag formula $\tau \approx \sqrt{|V(\mathbf{r}(t_0))|/n_f}/E_0$ in the TRCM is determined by the basic laser and atomic parameters and is independent of the observable. Substituting the relation $r(t_0) \approx I_p/E_0$ into the above expression for τ, we also arrive at the scaling law in Eq. (13). As this lag cannot be directly measured in experiments, it can be deduced from an observable, such as the angle θ according to the mapping in Eq. (4) or the approximate one in Eq. (6). It is worth noting that for small ellipticity ε, the interference of the rescattering electron and the direct electron will remarkably affect the PMD (as discussed in Fig. 2) and therefore affect the resolution of the offset angle as well as the time deduced from the angle. However, the rescattering plays a small role in this lag itself. As shown in Fig. 3, the lag calculated with Eq. (7) is similar to that evaluated with TDSE simulations.

Time lag. In Fig. 3, we further compare the ionization time lags obtained with different methods. Unlike the offset angle, which is related to the PMD and therefore can be directly measured in experiments, the lag is related to the instantaneous ionization property of the laser-driven system, which is not easy to probe in experiments. However, in TDSE simulations, this lag can be evaluated by approximately calculating the instantaneous ionization rate. Specifically, we first find the time t_i which corresponds to the maximal value of the instantaneous ionization rate $P(t) = dI(t)/dt$ [33]. Here, $I(t) = 1 - \sum_n |\langle n|\Psi(\mathbf{r}, t)\rangle|^2$ is the instantaneous ionization yield, $|n\rangle$ is the bound eigenstate of the field-free Hamiltonian H_0, and $|\Psi(\mathbf{r}, t)\rangle$ is the TDSE wave function of $H(t)$. We consider only the first several bound eigenstates with $n = 0, 1, 2, \ldots, 5$. The upper limit of n, n_u, is determined by the eigenenergy E_{n_u+1} of the $(n_u + 1)$th eigenstate, approximately agreeing with the semiclassical analysis. That is, $E_{n_u+1} \approx V(\mathbf{r}(t_0))$. Then the lag τ is obtained with $\tau = t_i - t_0$, where t_0 is the neighboring peak time of the laser field, agreeing with $|E_x(t_0)| = E_0$. We mention that the value of t_i evaluated here depends on the number $n' = n_u + 1$ of bound states excluded from $|\Psi(\mathbf{r}, t)\rangle$. Our simulations show that when the number n' is larger, the time lag obtained is also larger. However, despite this dependence, the appearance of a nonzero τ at different numbers n' suggests that at a certain time t_0, the electronic wave packet which leaves the ground state does not appear at the continuum state instantly, and therefore, the maximal ionization rate also does not appear at the peak time of the laser field. In particular, as shown in the following, with a definition of ionization similar to the TRCM, the TDSE prediction of τ is comparable to the TRCM one.

In addition to comparing the TDSE results to the TRCM predictions in Eq. (7), we also compare them to the CCAC predictions in Eq. (6) with $\tau \approx \varepsilon\theta/\omega$, where the offset angle θ is obtained from the PMD of the TDSE.

First, we can observe from Fig. 3 that the TDSE results for the lag τ increase with the increase of ellipticity. In addition, the TDSE results for different wavelengths at a certain value of ellipticity are comparable when $\varepsilon \leqslant 0.6$, and they begin to differ somewhat from each other for $\varepsilon > 0.6$, with the case of shorter wavelengths showing larger τ. The trends for both the parameter regions $\varepsilon \leqslant 0.6$ and $\varepsilon > 0.6$ are well reproduced by the TRCM. In particular, the quantity of the TDSE lag is comparable to the TRCM one, with a difference smaller than 10 as. These ellipticity-dependent phenomena for the angle θ can also be understood with Eq. (13). It should be noted that Eq. (13) is independent of the laser wavelength λ, but the TDSE and TRCM results in Fig. 3 show a weak dependence on λ for larger ε. The reason is that Eq. (13) uses the approximation $r(t_0) \approx I_p/E_0$, which neglects the effect of the laser wavelength. By comparison, Eq. (7), which is used to obtain the TRCM results shown here, includes the influence of $\lambda \sim 1/\omega$.

Second, the CCAC results differ from the TDSE and TRCM ones for $\varepsilon \leqslant 0.6$ and get close to them for $\varepsilon > 0.6$. Since the CCAC lag τ is obtained with the TDSE offset angle, the angle differences between the TDSE and TRCM in Fig. 2(c) for smaller ellipticity also shed light on the corresponding lag differences between the CCAC and TRCM in Fig. 3.

Third, unlike the remarkable difference between the TDSE and TRCM for the momentum component p_x at smaller ε seen in Fig. 2(b), the predictions of TDSE and TRCM for the lag are comparable at different ellipticities in Fig. 3. This suggests that the TRCM is capable of providing a good description of time-resolved ionization dynamics at different laser ellipticities. The offset angle and the momentum p_x related to this angle are possibly influenced by other effects such as quantum interference between different electron trajectories at small ellipticity [9]. As a result, the comparison between the TDSE and TRCM for this angle or the momentum p_x could also be influenced.

Three-dimensional cases. In Fig. 4, we further compare the predictions of the TRCM to the results of the 3D TDSE and experiments. It is worth noting that with Eq. (7), this lag is smaller in the 3D cases than in the 2D ones with similar laser and atomic parameters, and so is the offset angle. From Fig. 4(a), we can see that the results for the TRCM, 3D TDSE, and experiments for p_y agree well with each other. They show that the value of p_y increases remarkably with the increase

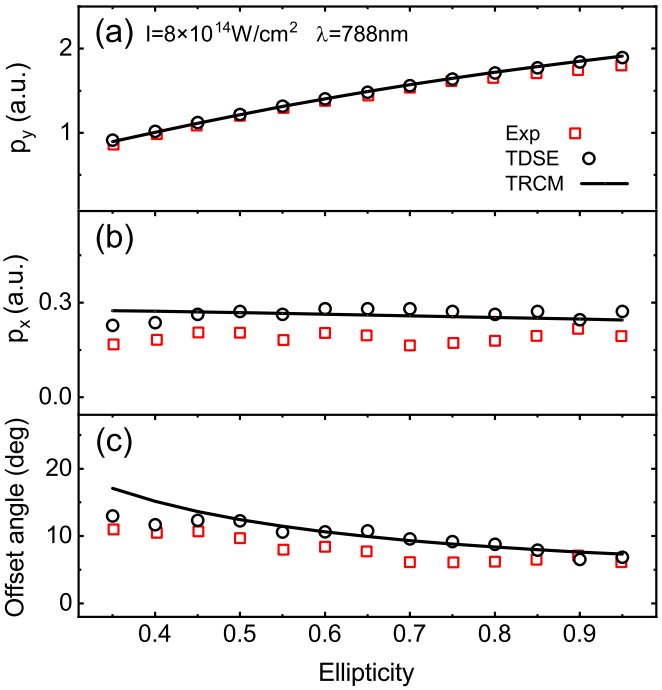

FIG. 4. Comparisons of the drift momentum (p_x, p_y) related to the MPR and the offset angle θ for experiments [26], the 3D TDSE, and the TRCM from Eq. (4) at different laser ellipticities ε. In (c), the experimental offset angles are obtained with $\theta \approx \arctan(p_x/p_y)$. Laser parameters are $I = 8 \times 10^{14}$ W/cm^2 and $\lambda = 788$ nm.

of ellipticity. For the case of p_x in Fig. 4(b), the results for the TRCM and 3D TDSE are also in good agreement with each other for $\varepsilon \geqslant 0.45$ but differ somewhat from each other for $\varepsilon < 0.45$. They also differ from the experimental results for different ellipticities with a difference of $\triangle p_x \approx 0.07$ a.u. Despite this difference, all of the results in Fig. 4(b) show that the value of p_x almost does not change with the increase in ellipticity, similar to the 2D cases. The comparisons in Fig. 4(c) for the offset angle are somewhat similar to the cases for p_x in Fig. 4(b), but the angle curves show a clear decreasing trend with the increase in ellipticity in Fig. 4(c). Although the TRCM and 3D TDSE results are also consistent with each other for $\varepsilon \geqslant 0.45$, they are somewhat higher than the experimental ones, with a difference of about 1° to 2°. The above ellipticity-dependent phenomena can also be well understood with the scaling laws in Eqs. (11) and (12). The difference between the TDSE and model results and experiments may partly arise from the uncertainty in the laser intensity used in experiments. Experiments for more targets are highly desired to further validate these ellipticity-dependent phenomena.

IV. FURTHER DISCUSSION OF TIME LAG

In the general attoclock procedure [40], the offset angle θ is considered to include two parts: θ_{delay}, which is related to the tunneling time delay, and θ_{ref}, which arises from the Coulomb-induced deflection when the tunneling electron moves far away from the nucleus. In our theory, the whole offset angle θ is related to the Coulomb-induced ionization time lag τ, as shown by Eq. (6), and therefore, the tunneling time delay could also be the one included in this lag.

The reasons for calling this lag the Coulomb-induced ionization time lag are as follows.

(1) In our previous TDSE and model studies [33,41], the maximal instantaneous ionization velocity does not appear at the peak time t_0 of the laser field. Instead, it appears at a time $t_i = t_0 + \tau$ with a lag τ to t_0. By contrast, for a short-range potential, this lag disappears. So we call this lag the Coulomb-induced ionization time lag. Using this lag concept, we find that many complex strong-field phenomena can be understood easily [33,34,36,42,43], so we consider that this lag reflects an intuitive and essential physical time, namely, the response time of an electron inside an atom to light in strong-field ionization, or, quantum mechanically, the response time of the electronic wave function to a strong-field ionization event.

(2) Based on TDSE results, we propose a theory to quantitatively describe this lag which is called the TRCM [28]. In the TRCM, this lag is defined as the measurable time of the strong three-body interaction between the electron, Coulomb, and laser, which can be determined at the boundary between quantum and classical. Specifically, in the TRCM, it is considered that when the electron appears at the tunnel exit $\mathbf{r}(t_0)$ at the peak time t_0 of the laser field, it is not free instantly. Instead, the electron is located in a quasibound state which approximately agrees with the virial theorem. This quasibound state can be further treated as a quasiparticle with a velocity component v_x induced by the Coulomb potential. This velocity v_x satisfies the relation $|v_x| \approx \sqrt{|V(\mathbf{r}(t_0))|/n_f}$ and disappears for a short-range potential. Its direction points to the parent nucleus and is opposite the direction of the exit-position vector at t_0. An impulse $E_0\tau = -v_x$ with the interaction time $\tau = |v_x|/E_0$ is needed for the tunneling electron to offset the velocity v_x induced by the Coulomb potential. When the time is greater than $t_i = t_0 + \tau$, the influence of Coulomb potential can be neglected, and the electron is free.

(3) The above discussion shows that the Coulomb effect related to the presumed velocity v_x is responsible for the lag τ of the ionization time $t_i = t_0 + \tau$ relative to the tunneling-out time t_0 in the TRCM. In addition, the picture of this lag in the TRCM agrees with that in the TDSE simulations, and the quantity of this lag in the TRCM also agrees with the TDSE one (see Fig. 3), so we also call this lag the Coulomb-induced one as in the TDSE simulations. The derivation of the formula for this lag in the TRCM shows that this lag can also be understood as the intuitive response time of the electron bounded by the Coulomb potential in laser-induced tunneling ionization. So we call the lag τ the time of the strong three-body interaction, the Coulomb-induced ionization time lag, and the response time of laser-induced photoemission. These terms for this lag emphasize different aspects of this lag.

Using the lag calculated by basic laser and atomic parameters, the experimental observable (e.g., the offset angle) can also be deduced with a simple mapping in the TRCM, as shown by Eq. (4). The TRCM is able to quantitatively reproduce a series of recent attoclock experimental curves [17,20,22,23] by providing a consistent physical picture for phenomena observed in the experiments. So we consider that this lag, which reflects the essential response time, is general for strong-field ionization of atoms and molecules.

V. CONCLUSION

In summary, we have studied the ionization of He in strong elliptical laser fields with different laser ellipticities and wavelengths numerically and analytically. We have compared the TDSE results to predictions of a Coulomb-included strong-field model called the TRCM and to experiments. The calculated offset angle in the photoelectron momentum distribution decreases with the increase of laser ellipticity, in agreement with the experimental measurement and the model prediction. This phenomenon can be understood by analyzing the ellipticity dependence of the momentum components related to this angle, p_x and p_y. When the component p_x along the major axis of the laser polarization is not sensitive to ellipticity, the component p_y along the minor one increases remarkably with increasing ellipticity. With the TRCM model, the scaling laws of the momentum (p_x, p_y) and the angle θ to the ellipticity ε were also given and explain the ellipticity-dependent phenomena for these two momentum components and this angle. Because the momentum component p_x is closely associated with the Coulomb-induced ionization time lag, we also further discussed the dependence of this lag on ellipticity. We evaluated this lag with different methods, including the TDSE method, the TRCM method, and a mix of the TDSE and TRCM called the CCAC. These different methods give similar ellipticity-dependent results for the lag τ at larger ellipticity, indicating that one can deduce this lag from the offset angle measured in attoclock experiments.

ACKNOWLEDGMENTS

This work was supported by the National Natural Science Foundation of China (Grant No. 12174239) and the Fundamental Research Funds for the Central Universities of China (Grant No. 2021TS089).

[1] P. B. Corkum and F. Krausz, Attosecond science, Nat. Phys. **3**, 381 (2007).
[2] F. Krausz and M. Ivanov, Attosecond physics, Rev. Mod. Phys. **81**, 163 (2009).
[3] M. Schultze *et al.*, Delay in photoemission, Science **328**, 1658 (2010).
[4] J. M. Dahlström, A. L'Huillier, and A. Maquet, Introduction to attosecond delays in photoionization, J. Phys. B **45**, 183001 (2012).
[5] F. Lépine, M. Y. Ivanov, and M. J. J. Vrakking, Attosecond molecular dynamics: Fact or fiction, Nat. Photonics **8**, 195 (2014).
[6] R. Pazourek, S. Nagele, and J. Burgdörfer, Attosecond chronoscopy of photoemission, Rev. Mod. Phys. **87**, 765 (2015).
[7] J. Vos, L. Cattaneo, S. Patchkovskii, T. Zimmermann, C. Cirelli, M. Lucchini, A. Kheifets, A. S. Landsman, and U. Keller, Orientation-dependent stereo Wigner time delay and electron localization in a small molecule, Science **360**, 1326 (2018).
[8] B. Yang, K. J. Schafer, B. Walker, K. C. Kulander, P. Agostini, and L. F. DiMauro, Intensity-Dependent Scattering Rings in High Order Above-Threshold Ionization, Phys. Rev. Lett. **71**, 3770 (1993).
[9] W. Becker, F. Grasbon, R. Kopold, D. B. Miloevi, G. G. Paulus, and H. Walther, Above-threshold ionization: From classical features to quantum effects, Adv. At. Mol. Opt. Phys. **48**, 35 (2002).
[10] P. B. Corkum, Plasma Perspective on Strong Field Multiphoton Ionization, Phys. Rev. Lett. **71**, 1994 (1993).
[11] M. Lewenstein, Ph. Balcou, M. Yu. Ivanov, A. L'Huillier, and P. B. Corkum, Theory of high-harmonic generation by low-frequency laser fields, Phys. Rev. A **49**, 2117 (1994).
[12] P. Eckle, M. Smolarski, P. Schlup, J. Biegert, A. Staudte, M. Schöffler, H. G. Muller, R. Dörner, and U. Keller, Attosecond angular streaking, Nat. Phys. **4**, 565 (2008).
[13] P. Eckle, A. N. Pfeiffer, C. Cirelli, A. Staudte, R. Dörner, H. G. Muller, M. Büttiker, and U. Keller, Attosecond ionization and tunneling delay time measurements in helium, Science **322**, 1525 (2008).
[14] A. N. Pfeiffer, C. Cirelli, M. Smolarski, and U. Keller, Recent attoclock measurements of strong field ionization, Chem. Phys. **414**, 84 (2013).
[15] A. S. Landsman, M. Weger, J. Maurer, R. Boge, A. Ludwig, S. Heuser, C. Cirelli, L. Gallmann, and U. Keller, Ultrafast resolution of tunneling delay time, Optica **1**, 343 (2014).
[16] M. Klaiber, K. Z. Hatsagortsyan, and C. H. Keitel, Tunneling Dynamics in Multiphoton Ionization and Attoclock Calibration, Phys. Rev. Lett. **114**, 083001 (2015).
[17] L. Torlina, F. Morales, J. Kaushal, I. Ivanov, A. Kheifets, A. Zielinski, A. Scrinzi, H. G. Muller, S. Sukiasyan, M. Ivanov, and O. Smirnova, Interpreting attoclock measurements of tunnelling times, Nat. Phys. **11**, 503 (2015).
[18] N. Teeny, E. Yakaboylu, H. Bauke, and C. H. Keitel, Ionization Time and Exit Momentum in Strong-Field Tunnel Ionization, Phys. Rev. Lett. **116**, 063003 (2016).
[19] N. Camus, E. Yakaboylu, L. Fechner, M. Klaiber, M. Laux, Y. Mi, K. Z. Hatsagortsyan, T. Pfeifer, C. H. Keitel, and R. Moshammer, Experimental Evidence for Quantum Tunneling Time, Phys. Rev. Lett. **119**, 023201 (2017).
[20] U. S. Sainadh, H. Xu, X. Wang, A. Atia-Tul-Noor, W. C. Wallace, N. Douguet, A. Bray, I. Ivanov, K. Bartschat, A. Kheifets, R. T. Sang, and I. V. Litvinyuk, Attosecond angular streaking and tunnelling time in atomic hydrogen, Nature (London) **568**, 75 (2019).
[21] W. Quan, V. V. Serov, M. Z. Wei, M. Zhao, Y. Zhou, Y. L. Wang, X. Y. Lai, A. S. Kheifets, and X. J. Liu, Attosecond Molecular Angular Streaking with All-Ionic Fragments Detection, Phys. Rev. Lett. **123**, 223204 (2019).
[22] A. N. Pfeiffer, C. Cirelli, M. Smolarski, D. Dimitrovski, M. Abu-samha, L. B. Madsen, and U. Keller, Attoclock reveals natural coordinates of the laser-induced tunnelling current flow in atoms, Nat. Phys. **8**, 76 (2012).
[23] R. Boge, C. Cirelli, A. S. Landsman, S. Heuser, A. Ludwig, J. Maurer, M. Weger, L. Gallmann, and U. Keller, Probing

Nonadiabatic Effects in Strong-Field Tunnel Ionization, Phys. Rev. Lett. **111**, 103003 (2013).

[24] A. W. Bray, S. Eckart, and A. S. Kheifets, Keldysh-Rutherford Model for the Attoclock, Phys. Rev. Lett. **121**, 123201 (2018).

[25] A. N. Pfeiffer, C. Cirelli, A. S. Landsman, M. Smolarski, D. Dimitrovski, L. B. Madsen, and U. Keller, Probing the Longitudinal Momentum Spread of the Electron Wave Packet at the Tunnel Exit, Phys. Rev. Lett. **109**, 083002 (2012).

[26] A. S. Landsman, C. Hofmann, A. N. Pfeiffer, C. Cirelli, and U. Keller, Unified Approach to Probing Coulomb Effects in Tunnel Ionization for Any Ellipticity of Laser Light, Phys. Rev. Lett. **111**, 263001 (2013).

[27] M. D. Feit, J. A. Fleck, Jr., and A. Steiger, Solution of the Schrödinger equation by a spectral method, J. Comput. Phys. **47**, 412 (1982).

[28] J. Y. Che, C. Chen, W. Y. Li, S. Wang, X. J. Xie, J. Y. Huang, Y. G. Peng, G. G. Xin, and Y. J. Chen, Response time of photoemission at quantum-classic boundary, arXiv:2111.08491.

[29] M. Lewenstein, K. C. Kulander, K. J. Schafer, and P. H. Bucksbaum, Rings in above-threshold ionization: A quasiclassical analysis, Phys. Rev. A **51**, 1495 (1995).

[30] T. Brabec, M. Yu. Ivanov, and P. B. Corkum, Coulomb focusing in intense field atomic processes, Phys. Rev. A **54**, R2551(R) (1996).

[31] S. P. Goreslavski, G. G. Paulus, S. V. Popruzhenko, and N. I. Shvetsov-Shilovski, Coulomb Asymmetry in Above-Threshold Ionization, Phys. Rev. Lett. **93**, 233002 (2004).

[32] T. M. Yan, S. V. Popruzhenko, M. J. J. Vrakking, and D. Bauer, Low-Energy Structures in Strong Field Ionization Revealed by Quantum Orbits, Phys. Rev. Lett. **105**, 253002 (2010).

[33] X. J. Xie, C. Chen, G. G. Xin, J. Liu, and Y. J. Chen, Coulomb-induced ionization time lag after electrons tunnel out of a barrier, Opt. Express **28**, 33228 (2020).

[34] S. Wang, J. Y. Che, C. Chen, G. G. Xin, and Y. J. Chen, Tracing the origins of an asymmetric momentum distribution for polar molecules in strong linearly polarized laser fields, Phys. Rev. A **102**, 053103 (2020).

[35] L. V. Keldysh, Ionization in the field of a strong electromagnetic wave, Sov. Phys. JETP **20**, 1307 (1965).

[36] J. Y. Che, C. Chen, S. Wang, G. G. Xin, and Y. J. Chen, Measuring ionization time lag of polar molecules with a calibrated attoclock, New J. Phys. **25**, 013016 (2023).

[37] M. Abu-samha, and L. B. Madsen, Interrogation of orbital structure by elliptically polarized intense femtosecond laser pulses, Phys. Rev. A **84**, 023411 (2011).

[38] H. Xie, M. Li, S. Q. Luo, Y. Li, Y. M. Zhou, W. Cao, and P. X. Lu, Energy-dependent angular shifts in the photoelectron momentum distribution for atoms in elliptically polarized laser pulses, Phys. Rev. A **96**, 063421 (2017).

[39] M. Abu-samha, and L. B. Madsen, Probing atomic and molecular targets by intense bicircular counter-rotating laser fields, J. Phys. B **51**, 135401 (2018).

[40] C. Hofmann, A. S. Landsman, and U. Keller, Attoclock revisited on electron tunnelling time, J. Mod. Opt. **66**, 1052 (2019).

[41] S. Wang, J. Cai, and Y. J. Chen, Ionization dynamics of polar molecules in strong elliptical laser fields, Phys. Rev. A **96**, 043413 (2017).

[42] J. Y. Che, C. Chen, S. Wang, G. G. Xin, and Y. J. Chen, Characterizing subcycle electron dynamics of polar molecules by asymmetry in photoelectron momentum distributions, Phys. Rev. A **104**, 063104 (2021).

[43] X. J. Xie, R. H. Xu, F. B. Zhang, S. J. Yu, X. Liu, W. Li, and Y. J. Chen, Coulomb effects on time-trajectory-resolved high-order harmonic generation, J. Phys. B **55**, 185002 (2022).